ARTICLE

Correlative Fluorescence Microscopy and Scanning Transmission Electron Microscopy of Quantum-Dot-Labeled Proteins in Whole Cells in Liquid

Madeline J. Dukes,[†] Diana B. Peckys,[‡] and Niels de Jonge[§,*]

[†]Department of Chemistry, Vanderbilt University, Nashville, Tennessee 37235, [‡]Center for Environmental Biotechnology, University of Tennessee, Knoxville, Tennessee 37996-1605, and [§]Department of Molecular Physiology and Biophysics, Vanderbilt University School of Medicine, Nashville, Tennessee 37232, and Materials Science and Technology Division, Oak Ridge National Laboratory, Oak Ridge, Tennessee 37831-6064

ABSTRACT Correlative fluorescence microscopy and transmission electron microscopy (TEM) is a state-of-the-art microscopy methodology to study cellular function, combining the functionality of light microscopy with the high resolution of electron microscopy. However, this technique involves complex sample preparation procedures due to its need for either thin sections or frozen samples for TEM imaging. Here, we introduce a novel correlative approach capable of imaging whole eukaryotic cells in liquid with fluorescence microscopy and with scanning transmission electron microscopy (STEM); there is no additional sample preparation necessary for the electron microscopy. Quantum dots (QDs) were bound to epidermal growth factor (EGF) receptors of COS7 fibroblast cells. Fixed whole cells in saline water were imaged with fluorescence microscopy and subsequently with STEM. The STEM images were correlated with fluorescence images of the same cellular regions. QDs of dimensions 7 × 12 nm were visible in a 5 μm thick layer of saline water, consistent with calculations. A spatial resolution of 3 nm was achieved on the QDs.

KEYWORDS: scanning transmission electron microscopy · quantum dots · molecular probes · protein labels · correlative microscopy · fluorescence microscopy · electron microscopy in liquid

*Address correspondence to niels.de.jonge@vanderbilt.edu.

Received for review April 2, 2010 and accepted June 8, 2010.

Published online June 15, 2010.
10.1021/nn1010232

Cellular function is governed by the interaction of molecules with dimensions in the nanometer range, such as proteins, lipids, and DNA. Protein interactions in cells can be studied with fluorescence microscopy.[1] However, the spatial resolution is limited by diffraction to about 200 nm, and it is thus not possible to elucidate what happens at the level of individual molecules, for example, in protein complexes. Also, the recently introduced subdiffraction (nanoscopy) techniques[2] do not reach a resolution in the required nanometer range (<10 nm). Cellular ultrastructure is traditionally investigated at the nanoscale with transmission electron microscopy (TEM). TEM imaging requires the preparation of the cells into conventional thin sections or into cryosections.[3] The cells are thus not in their liquid state and not intact (note that TEM imaging can be accomplished on cryo samples at the very edge of intact cells). Correlative microscopy is a strategy, developed in the past decade, to combine the functionality of light microscopy with the high resolution of electron microscopy. By introducing fluorescent molecular probes, it is possible to image regions containing a protein of interest with fluorescence microscopy and then to investigate the underlying ultrastructure with TEM, after preparing a conventional thin section, or a cryosection, of the cell.[4] A certain intracellular process can first be followed with light microscopy, the cell can be fixed, or frozen at a time point of interest, and the sample can then be further studied with TEM.[5] Correlating light and electron microscopy also allows one to search for a region of interest with light microscopy prior to TEM imaging, thus reducing radiation damage induced by searching with TEM.[6] In addition to fluorescence labels, a second tag consisting of an electron-dense material, such as a gold, may be employed. The spatial distribution of a certain type of protein of interest can then be investigated at the nanometer scale with TEM.[7,8] It is also possible to use bimodal probes visible with both fluorescence and electron microscopy, such as dye-conjugated gold nanoparticles, or semiconductor nanocrystals, so-called quantum dots (QDs).[9] Different types of proteins can be labeled with QDs of different sizes exhibiting different fluorescence signatures.[10] Finally, electron-dense materials for contrast in TEM may be precipitated *via* photo-oxidation at the positions of fluorescent labels.[11] The key limitation in correlative fluorescence microscopy and TEM

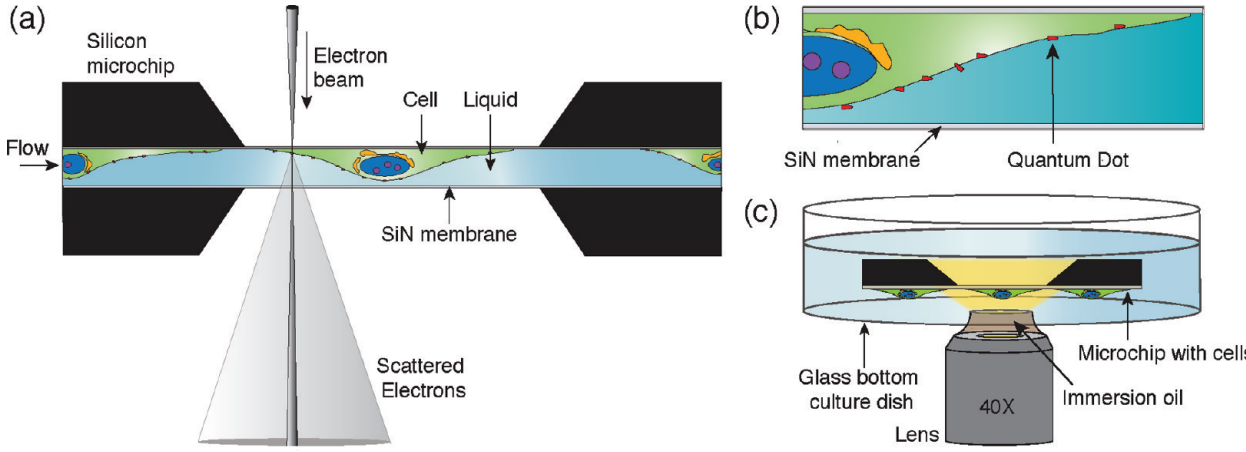

Figure 1. Schematic of the experimental setup for correlative light microscopy and liquid scanning transmission electron microscopy (STEM). Images are not drawn to scale. (a) Microfluidic chamber for liquid STEM consisting of two microchips each supporting an electron transparent window. Cells are directly grown on the top microchip. The bottom microchip contains a spacer (not shown). This chamber is placed in the vacuum of the STEM and imaged with a scanning electron beam. Transmitted electrons are detected. (b) Contrast is obtained in liquid STEM on nanoparticles specifically attached to surface proteins of the cell. (c) For imaging with light microscopy, prior to liquid STEM imaging, the microchip with the attached cells is placed upside-down in a glass bottom culture dish and imaged using an oil immersion lens.

is the need for thin sections, or for cryo samples, which complicates experimental procedures and is prone to introducing artifacts.

We have recently introduced a novel electron microscopy technique for imaging whole eukaryotic cells in liquid[12] or in a wet environment.[13] Eukaryotic cells in liquid are placed in a microfluidic chamber with a thickness of up to 10 μm contained between two ultrathin and electron-transparent windows (see Figure 1a). The specimen is then imaged with a scanning transmission electron microscope (STEM). Due to the atomic number (*Z*) contrast of the annular dark-field (ADF) detector of the STEM, nanoparticles of a high-*Z* material, such as gold, can be detected within the background signal produced by a micrometers-thick layer of a low-*Z* liquid, such as water. Specific protein labels consisting of nanoparticles can then be used to study the locations of individual proteins in whole cells in liquid. In our initial work,[12,13] surface receptors were labeled with gold nanoparticles and a spatial resolution of 4 nm was achieved.

Here we show that liquid STEM can be used to image QDs bound to surface proteins of eukaryotic cells, and that the STEM images can be correlated with fluorescence images. We also evaluate the signal-to-noise ratio of the liquid STEM images of QDs and determine the achievable resolution. The imaging methodology introduced here allows the imaging of whole fixed cells in liquid with both fluorescence and electron microscopy. There is no additional sample preparation necessary for the electron microscopy. Cells are grown and labeled directly on the microchips of the microfluidic device. Prior to and after fixation, the samples can be imaged with fluorescence microscopy. Subsequently, the same sample is assembled into a microfluidic system and imaged with STEM, with only a few minutes delay with respect to the first light microscopic imaging.

RESULTS AND DISCUSSION

Correlative Fluorescence Microscopy and Liquid STEM of QD-Labeled Cells. COS7 fibroblast cells were grown on silicon microchips with electron transparent windows for liquid STEM imaging.[12] The cells were incubated for 5 min at room temperature with epidermal growth factor (EGF) conjugated to QD (EGF-QD) and then fixed with glutaraldehyde. The incubation with EGF-QD and the fixation were done directly on the microchips. The cells on one microchip were imaged with light microscopy with the microchip placed upside-down in a cell culture dish with phosphate buffered saline water (see Figure 1c). Figure 2a shows a direct interference contrast (DIC) image and overlaid fluorescence image of a window section partly covered with adhered cells. The cells have flattened-out on the silicon nitride surface of the microchip. The DIC signal is visible through the silicon nitride window only, while the fluorescence signal is visible over the whole surface. The fluorescence signal is co-located with cellular material visible in the DIC signal. Figure 2b shows the fluorescence image separately. The QD labels light up as bright spots against a dark background of regions without cells. The cellular regions contain a faint fluorescence signal from the glutaraldehyde fixative. Bright spots indicate the locations of single QDs and/or bigger clusters of QDs, distributed over the entire surface of the cell, as expected for the used incubation time.[14] The image of Figure 2b was also used to locate the position of the cell with respect to the window, in order to correlate the light microscope and STEM images. Fluorescence and DIC images were recorded for six other samples.

Selected microchips with labeled cells in the window region were assembled into microfluidic cham-

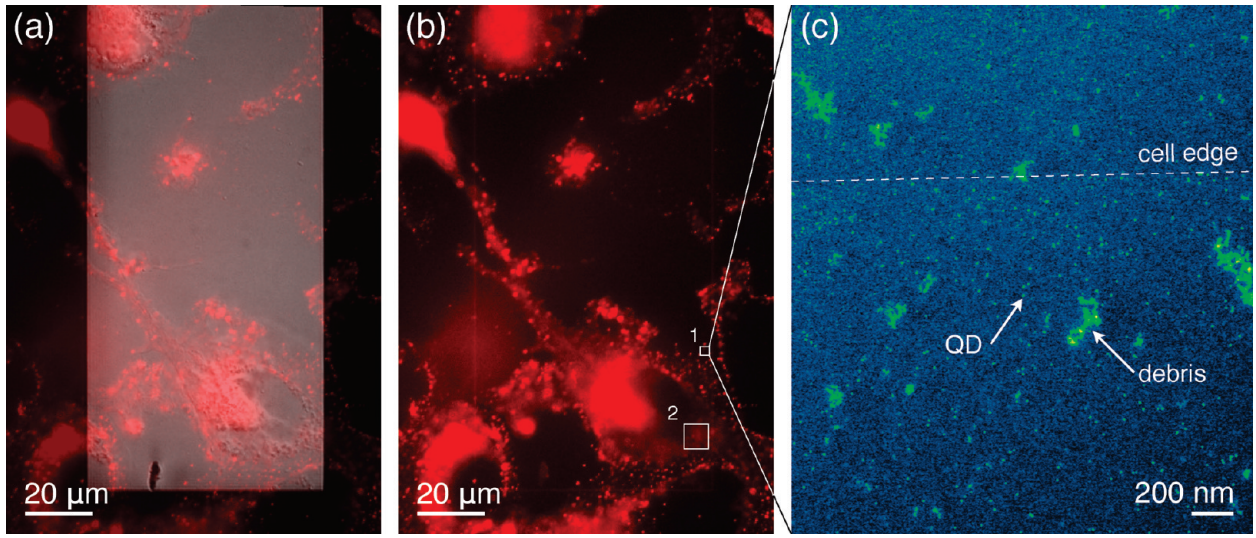

Figure 2. Correlative light microscopy and liquid STEM of intact fixed eukaryotic cells in saline water. (a) Direct interference contrast (DIC) image (gray) with overlaid fluorescent signal (red) of a microchip with COS7 cells showing the regions with quantum dot (QD)-labeled epidermal growth factor (EGF) receptors. The rectangular shape outlines the silicon nitride window. (b) Fluorescent signals (red) showing cellular regions with EGF receptors. Some fluorescence from the fixative is also visible. (c) Liquid STEM image of the region indicated with a square #1 in (b). Individual QDs along the edge of the cell can be discerned as yellow spots on a blue background. Some debris can be seen, as well. The magnification was $M = 48\,000$. The signal intensity was color-coded to increase the visibility of the labels.

bers for liquid STEM and imaged with a 200 kV STEM at a magnification $M = 48\,000$, while a continuous flow of buffer was maintained over the cells. Figure 2c shows a STEM image recorded at the edge of the same cell in the fluorescence image in Figure 2b. The lower two-thirds of the image contains bright spots of similar sizes that we associate with the presence of QDs. These bright spots are absent in the upper part of the image. We interpret the indicated transition line as the edge of the cell. Some debris from the microchip processing is visible, as well. Similar debris material was observed incidentally on microchip windows before cells were seeded and is residual material from the microchip processing that was not entirely washed off.

The QD-labeled EGF receptors were distributed almost evenly over the surface of the cell, consistent with the well-known behavior of the EGF receptor. Prior to EGF binding, the EGF receptor is known to be homogeneously distributed on the plasma membrane, as was shown by others *via* thin section TEM imaging of ferritin-labeled EGF[15] and of immuno-gold-labeled EGF receptors.[16] Incubation with EGF leads to ligand binding, activation of the receptor, and eventually internalization of the receptor *via* the formation of endocytocic vesicles after typical incubation times on the order of 30 min at room temperature.[14] The distribution of the labels thus changes with time from a homogeneous distribution to clusters of labels. The receptor distribution cannot be studied at the single-receptor level using fluorescence microscopy, so a microscopy technique with a resolution in the nanometer range is needed, for which traditionally TEM on thin sections is used. Figure 2c demonstrates that liquid STEM imaging provides information about the distribution of the individual EGF receptors correlated with the fluorescence image.

To verify the presence of liquid in the microfluidic chamber, we have determined the fraction, N/N_0, of electrons in the probe, N_0, scattered onto the ADF detector by the liquid in the microfluidic chamber. A fraction of $N/N_0 = 0.44$ was measured during imaging. The thickness of the liquid T follows from this fraction as[12]

$$T = -I(\beta)\ln\left(1 - \frac{N}{N_0}\right) \qquad (1)$$

with $I(\beta)$ being the mean free path length for elastic scattering in opening semiangle β or larger. Equation 1 assumes that most of the signal in the ADF detector is formed by single elastic scattering events and thus neglects multiple scattering and inelastic scattering. It was demonstrated in a recent study that the values of T obtained with eq 1 were accurate within 30% compared to thickness measurements performed *via* tilting the sample.[17] Water has $I_{water} = 10.5$ µm for $\beta = 70$ mrad.[12] Note that the mean free path length for the total elastic cross section (scattering by angles of $0-\pi$) for water at 200 kV is 0.43 µm, but most scattering events lead only to minor angular changes of the electron trajectories and do not cause electrons to scatter into the ADF detector. The larger mean free path length for the partial elastic cross section (scattering by angles of $\beta-\pi$) applies for angular changes sufficient to scatter electrons into the opening angle of the ADF detector. The value of I_{water} approximately equals the value of the buffer solution used here. The thickness of the liquid at the position of Figure 2b was calculated to be 6 $\pm$ 1 µm. This number is smaller than the diameter of

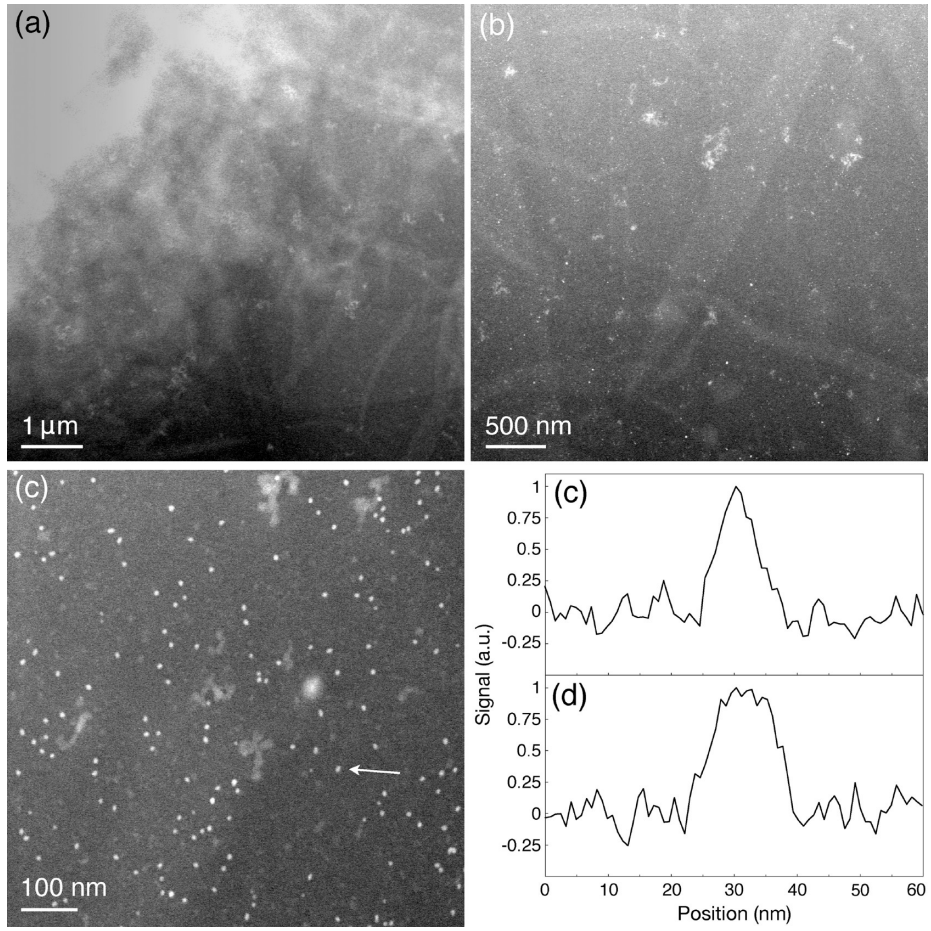

Figure 3. Liquid STEM images of a COS7 cell labeled with EGF-QD. (a) Cellular region at the position of the square #2 in Figure 2b recorded at $M = 16\,000$. (b) Image recorded at a region just at the bottom of the figure in (a) at $M = 32\,000$. QDs are visible as bright spots. (c) Image recorded at $M = 160\,000$ revealing the shape of the QDs. (d) Line scan over the QD indicated with the arrow in (c) over the short dimension of the QD. (e) Line scan over the same QD as in (d), but over the long dimension. The background level was set to zero.

the applied microspheres serving as spacer between the two microchips. Presumably, a compression of the microspheres occurred.

Localizing the same region in both a light and an electron microscopy image often requires dedicated procedures in correlative microscopy.[18,19] For liquid STEM, the localization was accomplished with a simple procedure as described in the following. The positions of features in the fluorescence image were measured with respect to the frame of the SiN window, visible in Figure 2a as rectangular shape and visible as a thin line in Figure 2b. Because the magnification used for the STEM imaging was too high to display the entire window area, the position of one corner of the SiN window was located first. The stage position at this point was recorded, and the scan rotation was aligned such that the scan direction of the electron beam ran parallel to the short side of the SiN window. During STEM imaging, the stage position of each image was recorded and correlated with the prior determined frame position of the SiN window. The position of Figure 2c corresponds to the square #1 in Figure 2b. The position of the square in the fluorescent image is at the edge of the cell, consistent with the finding of a separation line between regions with and without QDs in Figure 2c, interpreted as a cell edge.

A second region of the same cell is shown in square #2 of Figure 2b. Several STEM images were recorded in this area. Figure 3a shows an image recorded at $M = 16\,000$. The thickness of the liquid at this position was measured to be 5 ± 1 µm, consistent with the thickness determined for the region of Figure 2b within the accuracy of the measurement. The cellular material is visible as white irregular shapes, and the signal intensity increases toward the upper left corner to a level where the detector clipped. Cellular material has a shorter I value than water ($I_{cell} < I_{water}$) due to the higher average density and the higher average atomic number of protein, lipid, and DNA. Thus, a cellular region with a high density of protein, lipid, or DNA is expected to produce more scattering than water. The region in the upper left corner of Figure 3a can thus be interpreted as a region of the cell where it is denser or thicker than in the remaining region. This finding is consistent with the fluorescence image of Figure 2b, where the square #2 is located in proximity to the nucleus. It can thus be

concluded that correlative fluorescence microscopy and liquid STEM was accomplished on QD-labeled EGF receptors in whole COS7 cells in liquid. STEM images of two other samples also showed QDs in the cellular regions of the corresponding fluorescence image.

Resolving the Shape of the QDs. Liquid STEM images were recorded at higher magnifications, as well, to determine the shape of single QDs. Figure 3b was recorded at $M = 32\,000$, where some of the cellular material can still be discerned and the QDs are visible as small bright spots. Figure 3c, recorded at $M = 160\,000$, reveals the oval shape of the individual QDs. While the cellular material cannot be distinguished anymore, some of the debris is visible. A third type of object is the larger oval shape, center right, which is caused by electron beam contamination; that is, it appeared during imaging. The QD at the arrow was further analyzed. The line profile over the short dimension is shown in Figure 3d with a full width at half-maximum (fwhm) of 7 nm. The line profile over the long dimension has a fwhm of 12 nm, as shown in Figure 3e. The oval shape of the QDs was also detected by others, and STEM images at atomic resolution showed a bullet-like shape of QDs of the CdSe/CdZnS core/shell materials[20] that are used by the supplier (Invitrogen).

A total of 10 QDs was analyzed *via* line scans over their small dimensions, and it followed that the average fwhm was 8 ± 1 nm. The measured fwhm of the small dimension is consistent with the size of the CdSe core (~7.3 nm) surrounded by a ZnS shell, which adds an additional 1−2 nm.[20,21] The protein coating of the QDs is not visible in the STEM image due to the lower atomic number of this material compared to the core, and the resulting lower contrast in STEM. It can thus be concluded that QDs were indeed observed with liquid STEM and that the resolution was sufficient to resolve the oval shape of the QDs in a 5 μm thick layer of water (buffer).

Evaluation of the Signal-to-Noise Ratio of the Liquid STEM Images. The signal-to-noise-ratio (SNR) of the peak of the signals at the QD with respect to the background level was 9 ± 1. The noise level was the standard deviation of the signal in a line scan over the background near the QD. The experimental SNR can be compared with a theoretical prediction. From the equations for elastic scattering[22] and assuming 100% detection efficiency, it follows for the imaging of QDs in several micrometers of water that the noise-limited spatial resolution, d, obtained on the QDs is[12,17]

$$d = \mathrm{SNR}\, l_{\mathrm{QD}} \sqrt{\frac{T}{N_0 l_{\mathrm{water}}}} \qquad (2)$$

This equation gives the relationship between the QD size and the SNR in the image. With the density of the CdSe core of 5.8 g/cm^3,[23] and a molecular weight of 14 g/mol, it follows that $l_{\mathrm{QD}} = 0.40$ μm. Equation 2 predicts QDs with $d = 9$ nm to be visible with SNR = 9 for $T = 5$ μm and the microscope settings used here. This theoretical value corresponds to the experimental fwhm values of 7 and 12 nm for the short and long side, respectively. The fwhm is a measure of the size of the QD but is not necessarily equal to the actual diameter. The line scan represents a convolution of the object with the electron probe from the STEM imaging, but for our microscope settings, the electron probe size was about 0.6 nm, measured as the diameter containing 50% of the current, d_{50}, and the fwhm can be considered as a sufficiently accurate measure of a QD dimension. It can thus be concluded that the theoretical model predicts the outcome of the measurements within the accuracy of the measurements and of eq 2.

Resolution of Liquid STEM on QDs. We have also determined the spatial resolution achieved in this experiment. For a situation where the electron probe is much smaller than the imaged object, a measure often used to determine the spatial resolution is the 25−75% edge width, r_{25-75}.[24] Values of r_{25-75} were measured from the line scans over the QDs. Each r_{25-75} was determined from the average of the opposite edges of a line scan over the QD. The values of r_{25-75} for the QD of Figure 3d amounted to $r_{25-75} = 3$ nm. This value was the same for line scans over the long and short dimensions. The average over the small dimension of 10 QDs was 3.0 ± 0.5 nm. Thus, the spatial resolution achieved with liquid STEM of QDs on cells in buffer for $T = 5$ μm was 3 nm. This estimate applies for QDs in the upper region of the specimen with respect to the beam entrance. Interactions of the electron beam with the water will lead to beam broadening. At a depth of 0.5 μm, the electron probe will have increased to 4 nm,[12,17] still providing sufficient resolution, but at a depth of 1 μm, the probe size will be 9 nm and the QDs will be on the onset of visibility. QD-labeled receptors can thus be detected in many sections of the cells flattened on the silicon nitride membrane.

Biological electron microscopy is mostly limited by electron beam damage, and the resolution is then not limited by the electron probe size, but rather by the available electron dose. The minimum size d of a nanoparticle that can be resolved with a certain electron dose is calculated with eq 2. The Rose criterion[25] sets the limit SNR = 5, and the electron dose determines N_0. The pixel size in Figure 3c was 0.85 nm, larger than the d_{50}, and the electron dose was thus ~1.0×10^5 electrons/nm^2. This value is an order of magnitude larger than the limit of 8.0×10^3 electrons/nm^2 used in cryo-TEM of whole cells[26] and about a factor of 4 less than the limit used for the imaging of conventional thin sections.[27] A dose of 7×10^4 electrons/nm^2 applies for STEM imaging of fixed cells in liquid.[12] An electron dose of 1.0×10^5 electrons/nm^2, SNR = 5, and $T = 5$ μm, yield $d = 5$ nm. QDs with a smallest dimension of 5 nm would thus be visible with sufficient SNR for detection.

Difference between STEM and TEM. The STEM has a key advantage over TEM when imaging molecular labels of heavy materials, such as gold nanoparticles or quantum dots, and the obtained images are different than those obtained with TEM. The molecular labels are visible with high contrast, while the underlying ultrastructure is visible with much less contrast than in TEM. This "absence" of information has the advantage that the background levels are relatively low, thus promoting the visibility of the labels when imaging whole cells. The difference between STEM and TEM has its analogue in light microscopy, where fluorescence microscopy is used to image specifically labeled proteins and, for example, phase contrast is used to image the cellular structure. Correlative fluorescence microscopy and liquid STEM thus provides different information than correlative microscopy involving TEM.

CONCLUSIONS

These results demonstrate that liquid STEM is capable of imaging individual QDs used as specific protein labels on whole eukaryotic cells in liquid, and that the liquid STEM images can be readily correlated with their fluorescent counterparts. The sample preparation method used for liquid STEM is similar to standard methods used for light microscopy with the difference that nanoparticle labels of heavy materials are needed to provide contrast in STEM. Liquid STEM has two key advantages over state-of-the-art correlative light microscopy and TEM, requiring thin sections, or thin frozen samples: (1) Artifacts introduced by dehydration, post-staining, freezing, or sectioning are avoided. (2) In liquid STEM, cells are labeled live and fixed, after which no further sample processing is required. As a consequence, fluorescence microscopy can be used to monitor tagged proteins in living cells to determine the desired time point of the fixation. It is thus possible to examine a certain specific state of the cell by subsequent liquid STEM imaging. Currently, liquid STEM is limited to surface proteins and proteins that internalize as was shown for the EGF receptor,[12] but strategies for introducing nanoparticles into live cells, such as membrane penetrating peptides,[28] may be used to label intracellular proteins in the future. The spatial resolution of 3 nm demonstrated here is sufficient to discriminate nanoparticles differing in size, shape, and electron density for multilabel experiments to study the constituents of protein complexes within cells.

MATERIALS AND METHODS

Preparing the Microchips with COS7 Cells. COS7 (African green monkey fibroblast) cells were grown directly on the silicon microchips for the microfluidic chamber of the liquid STEM system.[12] Each microchip (2.60 × 2.00 × 0.30 mm) supported a silicon nitride window of a 70 × 200 μm area and 50 nm thickness (Protochips Inc.). The protective resist coating of the microchips was stripped by rinsing with acetone and subsequent rinsing with ethanol. The microchips were then plasma cleaned to render the surfaces hydrophilic and coated with poly-L-lysine to enhance cell adherence and to maintain the hydrophilic surface. COS7 cells were grown in Dulbecco's modified Eagle medium (DMEM) (Gibco) supplemented with 10% fetal bovine serum (FBS) (Sigma), penicillin/streptomycin antibiotics (100 units/mL and 100 μg/mL, Gibco), and additional L-glutamine (2 mM, Gibco) at 37 °C in a 5% CO_2 atmosphere. Confluent COS7 cells were harvested by rinsing in Dulbecco's phosphate buffered saline (PBS) and dissociating the adherent layer with CellStripper (Mediatech), followed by a quench in supplemented media. The cells were seeded onto the microchips and incubated in medium at 37 °C and 5% CO_2 for 1 day. Prior to labeling, the cells were incubated in serum-free medium for 4 h at 37 °C and 5% CO_2.

Preparing the Spacer Microchips. Each microfluidic chamber for liquid STEM consisted of a microchip with cells and a second microchip with spacers to provide a gap between the microchips for the specimen and for liquid flow. The microchips to be used with the spacer were first stripped of their protective coating with acetone and ethanol. While the surfaces were still hydrophobic, 0.2 μL droplets of an 8 μm diameter polystyrene microsphere suspension in water were pipetted onto the four corner regions of each microchip. The droplets of the suspension were dried, leaving the microspheres stuck to the four corners of the microchips' surfaces. The chips were then plasma cleaned to render the surfaces hydrophilic and coated with poly-L-lysine.

EGF-QD Labeling. QDs were coupled to EGF molecules *via* biotin−streptavidin binding.[14] The EGF-QD complexes were formed by incubating EGF-biotin (Invitrogen) in a 6:1 molar ratio with streptavidin-QD655 (Invitrogen) for 2 h at room temperature in a solution of 1.3 μM QD in 50 mM borate buffer, pH 8.3 (the QD stock solution was first centrifuged to remove aggregates). Free EGF-biotin was removed with a microcentrifuge purification column (Ultracel-100YM, Millipore). For specific labeling of the EGF receptors, the cells were incubated with 5 nM EGF-QD655 in Tyrode's buffer (Sigma), supplemented with 0.1% BSA (Sigma) and 50 mM D-glucose (Sigma-Aldrich) for 5 min at room temperature by immersing the microchips in incubation liquid.[12] The cells were then washed three times in PBS (Gibco) and fixed for 20 min with 4% glutaraldehyde in PBS. After fixation, the cells were washed three times with PBS and once in 10% PBS. The aldehydes in the fixative were quenched by incubating the microchips in 100 mM glycine in 10% PBS, followed by three rinses of the microchips in 10% PBS. Two different control experiments confirmed specific EGF labeling with QDs. The first control started with the above-described labeling of the cells with EGF-QDs. The control samples were then desalted, dried, and imaged with transmission electron microscopy (TEM). It was found that QDs were co-located with regions of the microchips containing cellular material. The second control involved the incubation with QD655-streptavidin without EGF-biotin. This control was also desalted, dried, and imaged with transmission electron microscopy (TEM). Only a very low amount of nonspecifically bound QDs was found.

Light Microscopy. The microchips with the labeled cells were placed upside-down in a 35 mm culture dish with thin glass bottom (Mat-tek), containing 2 mL of 10% PBS in water. Direct interference contrast (DIC) and fluorescent images (5 s exposure time) were recorded with a 40× oil immersion objective using a wide field microscope (TE300, Nikon) equipped with a far-red band-pass excitation filter (hq615/40 ×) and a far-red band-pass emission filter set (hq710/100 m). Fluorescence of the glutaraldehyde fixative was reduced prior to imaging by photobleaching, using the light source of the fluorescence microscope. The images were adjusted for optimum brightness and contrast, overlaid, and colored using ImageJ software (NIH).

Liquid STEM Imaging. For liquid STEM imaging, a microfluidic chamber containing a sample was assembled in a liquid specimen holder for STEM imaging (Protochips Inc.). This holder connected the specimen chamber to a syringe pump (Harvard Scientific) *via* microfluidic tubing (Upchurch Scientific). Before

assembly, the tubing was cleaned with purified water and then the slot for the microchips was dried. The spacer microchip was first loaded with the spacer facing up. A droplet of 0.5 μL 10% PBS was pipetted onto the surface, wetting it completely. The microchip with cells was then placed in the slot on the spacer microchip with the cells facing downward. The loading was done rapidly to prevent the chips from drying. The lid of the holder was then closed, the buffer solution was rinsed off the outer surface of the microchip to prevent the formation of a salt crust, and a 1−2 μL/min flow of 10% phosphate buffered saline (PBS) in water was initiated. The STEM (CM200, FEI Company, Oregon) was set to 200 kV, and a beam semiangle α of 11 mrad, a pixel dwell time of 20 μs, a probe current of 0.6 nA, a detector semiangle β of 70 mrad, and an image size of 1024 × 1024 pixels were chosen. The probe size containing 50% of the current was estimated to be $d_{50} = 0.6$ nm.[29] Contrast and brightness were adjusted for maximum visibility, and a convolution filter with a kernel of (1, 1, 1; 1, 5, 1; 1, 1, 1) was applied (using ImageJ) to reduce the noise in the STEM images; however, the data analysis *via* line scans was performed on the original, unfiltered data. The image of Figure 2c was recorded at the edge of the silicon nitride window where the window bulged in the vacuum toward the center of the window, resulting in a change of the background signal level as a function of the vertical coordinate. This increase in background signal was compensated for by using image processing (Digital Micrograph, Gatan).

Acknowledgment. We thank S. Head, T.E. McKnight, G.J. Kremers, E.A. Ring, D.W. Piston, and Proto-chips Inc. A portion of this research was conducted at the SHaRE User Facility, which is sponsored by the Division of Scientific User Facilities, Office of Basic Energy Sciences, U.S. Department of Energy. Research supported by Vanderbilt University School of Medicine, and by NIH Grant 1R43EB008589 (to S. Mick for D.B.P. and N.J.).

REFERENCES AND NOTES

1. Lippincott-Schwartz, J.; Snapp, E.; Kenworthy, A. Studying Protein Dynamics in Living Cells. *Nat. Rev.* **2001**, *2*, 444–456.
2. Hell, S. W. Far-Field Optical Nanoscopy. *Science* **2007**, *316*, 1153–1158.
3. Stahlberg, H.; Walz, T. Molecular Electron Microscopy: State of the Art and Current Challenges. *ACS Chem. Biol.* **2008**, *3*, 268–281.
4. Leis, A.; Rockel, B.; Andrees, L.; Baumeister, W. Visualizing Cells at the Nanoscale. *Trends Biochem. Sci.* **2009**, *34*, 60–70.
5. Sun, M. G.; Williams, J.; Munoz-Pinedo, C.; Perkins, G. A.; Brown, J. M.; Ellisman, M. H.; Green, D. R.; Frey, T. G. Correlated Three-Dimensional Light and Electron Microscopy Reveals Transformation of Mitochondria During Apoptosis. *Nat. Cell Biol.* **2007**, *9*, 1057–1065.
6. Sartori, A.; Gatz, R.; Beck, F.; Rigort, A.; Baumeister, W.; Plitzko, J. M. Correlative Microscopy: Bridging the Gap between Fluorescence Light Microscopy and Cryo-Electron Tomography. *J. Struct. Biol.* **2007**, *160*, 135–145.
7. Pombo, A.; Hollinshead, M.; Cook, P. R. Bridging the Resolution Gap: Imaging the Same Transcription Factories in Cryosections by Light and Electron Microscopy. *J. Histochem. Cytochem.* **1999**, *47*, 471–480.
8. Koster, A. J.; Klumperman, J. Electron Microscopy in Cell Biology: Integrating Structure and Function. *Nat. Rev. Mol. Cell Biol.* **2003**, ss6–ss10.
9. Gaietta, G.; Deerinck, T. J.; Adams, S. R.; Bouwer, J.; Tour, O.; Laird, D. W.; Sosinsky, G. E.; Tsien, R. Y.; Ellisman, M. H. Multicolor and Electron Microscopic Imaging of Connexin Trafficking. *Science* **2002**, *296*, 503–507.
10. Giepmans, B. N.; Deerinck, T. J.; Smarr, B. L.; Jones, Y. Z.; Ellisman, M. H. Correlated Light and Electron Microscopic Imaging of Multiple Endogenous Proteins Using Quantum Dots. *Nat. Methods* **2005**, *2*, 743–749.
11. Grabenbauer, M.; Geerts, W. J.; Fernadez-Rodriguez, J.; Hoenger, A.; Koster, A. J.; Nilsson, T. Correlative Microscopy and Electron Tomography of Gfp through Photooxidation. *Nat. Methods* **2005**, *2*, 857–862.
12. de Jonge, N.; Peckys, D. B.; Kremers, G. J.; Piston, D. W. Electron Microscopy of Whole Cells in Liquid with Nanometer Resolution. *Proc. Natl. Acad. Sci. U.S.A.* **2009**, *106*, 2159–2164.
13. Peckys, D. B.; Veith, G. M.; Joy, D. C.; de Jonge, N. Nanoscale Imaging of Whole Cells Using a Liquid Enclosure and a Scanning Transmission Electron Microscope. *PLoS One* **2009**, *4*, e8214.
14. Lidke, D. S.; Nagy, P.; Heintzmann, R.; Arndt-Jovin, D. J.; Post, J. N.; Grecco, H. E.; Jares-Erijman, E. A.; Jovin, T. M. Quantum Dot Ligands Provide New Insights into Erb/Her Receptor-Mediated Signal Transduction. *Nat. Biotechnol.* **2004**, *22*, 198–203.
15. McKanna, J. A.; Haigler, H. T.; Cohen, S. Hormone Receptor Topology and Dynamics: Morphological Analysis Using Ferritin-Labeled Epidermal Growth Factor. *Proc. Natl. Acad. Sci. U.S.A.* **1979**, *76*, 5689–5693.
16. Boonstra, J.; van Maurik, P.; Defize, L. H.; de Laat, S. W.; Leunissen, J. L.; Verkley, A. J. Visualization of Epidermal Growth Factor Receptor in Cryosections of Cultured A431 Cells by Immuno-Gold Labeling. *Eur. J. Cell Biol.* **1985**, *36*, 209–216.
17. de Jonge, N.; Poirier-Demers, N.; Peckys, D. B.; Drouin, D. Nanometer-Resolution Electron Microscopy through Micrometers-Thick Water Layers. *Ultramicroscopy*; doi:10.1016/j.ultramic.2010.04.001.
18. Keene, D. R.; Tufa, S. F.; Lunstrum, G. P.; Holden, P.; A., H. W. Confocal/TEM Overlay Microscopy: A Simple Method for Correlating Confocal and Electron Microscopy of Cells Expressing Gfp/Yfp Fusion Proteins. *Microsc. Microanal.* **2008**, *14*, 342–348.
19. Giepmans, B. N. G.; Deerinck, T. J.; Smarr, B. L.; Jones, Y. Z.; Ellisman, M. H. Correlated Light and Electron Microscopic Imaging of Multiple Endogenous Proteins Using Quantum Dots. *Nat. Methods* **2005**, *2*, 744–749.
20. McBride, J.; Treadway, J.; Feldman, L. C.; Pennycook, S. J.; Rosenthal, S. J. Structural Basis for near Unity Quantum Yield Core/Shell Nanocrystals. *Nano Lett.* **2006**, *6*, 1496–1501.
21. Yu, W. W.; Qu, L.; Guo, W.; Peng, X. Experimental Determination of the Extinction Coefficient of CdTe, CdSe, and CdS Nanocrystals. *Chem. Mater.* **2003**, *15*, 2854–2860.
22. Reimer, L. *Transmission Electron Microscopy*; Springer: Heidelberg, 1984.
23. Lee, B.; Kim, Y.; Lee, S.; Kim, Y. S.; Wang, D.; Cho, J. Layer-by-Layer Growth of Polymer/Quantum Dot Composite Multilayers by Nucleophilic Substitution in Organic Media. *Angew. Chem., Int. Ed.* **2010**, *49*, 359–363.
24. Reimer, L. *Scanning Electron Microscopy, Physics If Image Formation and Microanalysis*; Springer: Heidelberg, 1985.
25. Rose, A. Television Pickup Tubes and the Problem of Noise. *Adv. Electron.* **1948**, *1*, 131–166.
26. Iancu, C. V.; Wright, E. R.; Heymann, J. B.; Jensen, G. J. A Comparison of Liquid Nitrogen and Liquid Helium as Cryogens for Electron Cryotomography. *J. Struct. Biol.* **2006**, *153*, 231–240.
27. Luther, P. K.; Lawrence, M. C.; Crowther, R. A. A Method for Monitoring the Collapse of Plastic Sections as a Function of Electron Dose. *Ultramicroscopy* **1988**, *24*, 7–18.
28. Tkachenko, A. G.; Xie, H.; Liu, Y. L.; Coleman, D.; Ryan, J.; Glomm, W. R.; Shipton, M. K.; Franzen, S.; Feldheim, D. L. Cellular Trajectories of Peptide-Modified Gold Particle Complexes: Comparison of Nuclear Localization Signals and Peptide Transduction Domains. *Bioconjugate Chem.* **2004**, *15*, 482–490.
29. Barth, J. E.; Kruit, P. Addition of Different Contributions to the Charged Particle Probe Size. *Optik* **1996**, *101*, 101–109.